Published in final edited form as:
J Bone Miner Res. 2012 February ; 27(2): 486–495. doi:10.1002/jbmr.553.

Three-Dimensional Dynamic Bone Histomorphometry

C.R. Slyfield[1], **E.V. Tkachenko**[1], **D.L. Wilson**[2], and **C.J. Hernandez**[1]

C.R. Slyfield: crs256@cornell.edu; E.V. Tkachenko: et256@cornell.edu; D.L. Wilson: dlw@case.edu; C.J. Hernandez: cjh275@cornell.edu

[1]Biomedical Mechanics Laboratories, Sibley School of Mechanical and Aerospace Engineering and Biomedical Engineering, Cornell University, Ithaca, NY, USA

[2]Department of Biomedical Engineering, Case Western Reserve University, Cleveland, OH, USA

Abstract

Dynamic bone histomorphometry is the standard method for measuring bone remodeling at the level of individual events. While dynamic bone histomorphometry is an invaluable tool for understanding osteoporosis and other metabolic bone diseases, the technique's two-dimensional nature requires the use of stereology and prevents measures of individual remodeling event number and size. Here, we use a novel three-dimensional fluorescence imaging technique to achieve measures of individual resorption cavities and formation events. We perform this three-dimensional histomorphometry approach using a common model of postmenopausal osteoporosis, the ovariectomized rat. The three-dimensional images demonstrate the spatial relationship between resorption cavities and formation events consistent with the hemi-osteonal model of cancellous bone remodeling. Established ovariectomy was associated with significant increases in the number of resorption cavities per unit bone surface (2.38 ± 0.24 mm^{-2} SHAM v. 3.86 ± 0.35 mm^{-2} OVX, mean ± SD, $p < 0.05$) and total volume occupied by cavities per unit bone volume (0.38 ± 0.06% SHAM v. 1.12 ± 0.18% OVX, $p < 0.001$), but no difference in surface area per resorption cavity, maximum cavity depth, or cavity volume. Additionally, we find that established ovariectomy is associated with increased size of bone formation events due to merging of formation events ($23{,}700 \pm 6{,}890$ μm^2 SHAM v. $33{,}300 \pm 7{,}950$ μm^2 OVX). No differences in mineral apposition rate (determined in 3D) were associated with established ovariectomy. That established estrogen depletion is associated with increased number of remodeling events with only subtle changes in remodeling event size suggests that circulating estrogens may have their primary effect on the origination of new basic multicellular units with relatively little effect on the progression and termination of active remodeling events.

Keywords

Bone histomorphometry; Bone Remodeling; Osteoporosis; Ovariectomy; Rodent

Corresponding Author: Christopher J. Hernandez, Ph.D., 219 Upson Hall, Cornell University, Ithaca, NY 14853, Phone: (607) 255-5129, Fax: (607) 255-1222.

Disclosures: Dr. Wilson has an interest in BioInVision, Inc. which may commercialize the image acquisition/analysis approach. All other authors have no conflicts of interest.

Authors' Contributions: Study design: CRS and CJH. Data collection: CRS and EVT. Data analysis: CRS, EVT, and CJH. Data interpretation: CRS and CJH. Drafting manuscript: CRS, DLW, and CJH. Revising manuscript content: CRS, EVT, and CJH. Approval of final version of manuscript: CRS, EVT, DLW, and CJH. CJH takes responsibility for the integrity of the data analysis.

Conflicts of Interest: Dr. Wilson has an interest in BioInVision, Inc. which may commercialize the image acquisition/analysis approach. All other authors have no conflicts of interest.

Introduction

Bone remodeling is the primary process of modifying bone volume and microstructure in adults and is therefore a key process in the development and treatment of osteoporosis. Bone remodeling is a focal process that occurs at discrete locations on bone surfaces. An individual remodeling event is known as a basic multicellular unit (BMU). A basic multicellular unit consists of a group of osteoclasts that resorb bone followed in time by a group of osteoblasts that form bone [1]. In cancellous bone, the basic multicellular unit is believed to form a trench-like remodeling cavity on the bone surface referred to as a hemi-osteon [2]. The birthrate, number, and size of remodeling events determine the overall rate of bone turnover [3]. Because bone resorption precedes formation, each remodeling event is associated with the creation of a resorption cavity (Howship's lacuna). Resorption cavities on the surfaces of trabeculae are believed to generate stress concentrations that have a detrimental effect on the biomechanical performance of the entire cancellous bone structure [4]. Simple biomechanical analyses suggest that differences in the number and size (breadth and depth) of individual resorption cavities influence bone biomechanics [5,6].

Dynamic bone histomorphometry is the standard method for evaluating alterations in bone remodeling at the level of the basic multicellular unit [7,8]. Dynamic bone histomorphometry is unique in its ability to measure parameters such as the mineral apposition rate, bone formation rate and activation frequency [9]. In addition to measures of bone formation, bone histomorphometry studies typically include measures of bone volume fraction and percent eroded surface (ES/BS). Dynamic bone histomorphometry has provided key information regarding the development and treatment of osteoporosis and other metabolic bone diseases. However, measures of the size and number of remodeling events are not performed in traditional dynamic bone histomorphometry as they require labor intensive serial sections or specialized stereology techniques (the 'disector method') [9–11].

In our laboratory, we have advanced an imaging modality known as serial block face imaging [12,13]. Serial block face imaging can achieve three-dimensional images of bone and fluorescent markers of bone formation at a sub-micrometer scale [14,15]. We have previously demonstrated and validated approaches for visualizing bone surface texture and obtained measures of the number and surface size of resorption cavities (identified as eroded surfaces) in three-dimensional images [16]. Here we demonstrate an approach for three-dimensional measures of bone formation as well as resorption cavities and apply the approach to ovariectomized rats, the most commonly used animal model of post-menopausal osteoporosis.

Ovariectomy-induced estrogen depletion results in an increase in bone turnover in the rat, indicated by increases in mineralizing surface, osteoid surface, and eroded surface in cancellous bone present months after surgery [17,18]. It has been proposed that the increase in bone remodeling in established estrogen depletion is due to an increase in the birthrate of new remodeling events and extended progression of individual basic multicellular units across the bone surface, increasing both the number and surface area of individual remodeling events [2,19,20]. Traditional histomorphometry has provided detailed accounts of ovariectomy-induced estrogen depletion [21]. However, because remodeling events have not been observed and quantified in cancellous bone in three-dimensions, it is not known if established estrogen depletion consists of an alteration in the number or size of remodeling cavities; a subtle difference in bone remodeling that can alter local stress concentrations [5,6,22,23]. Additionally, it is not known how three-dimensional measures of bone formation (number and size of forming surfaces, mineral apposition rate, etc.) vary among remodeling sites or in established ovariectomy.

The overall goal of this line of investigation is to improve assessment of bone remodeling at the level of the individual remodeling event. We hypothesize that established estrogen depletion results in an increase in the number and size of resorption cavities and sites of bone formation. To test this hypothesis, we: 1) establish image processing and analysis methods to create three-dimensional images of bone formation markers and measures of resorption cavity depth and volume; and 2) determine the effect of established ovariectomy-induced estrogen depletion on the number and size of resorption cavities (identified as eroded surfaces), formation events, and mineral apposition rate at each formation event.

Materials and Methods

Image Acquisition

Ten, six-month-old female Sprague-Dawley rats were subjected to bilateral ovariectomy (OVX) or sham surgery (n=5 per group). Four months after surgery, the animals were euthanized and the fourth lumbar vertebrae were collected (these animals were part of a larger study examining drug treatment following established ovariectomy). This age group of animals was selected to characterize the condition of established estrogen depletion, after a new, post-ovariectomy steady state in bone remodeling is achieved. Animals were subjected to two doses of bone formation markers at 10 and 3 days prior to euthanasia (90 mg/kg xylenol orange followed by 10 mg/kg calcein). All animal use was approved by the Case Western Reserve University IACUC. Following euthanasia, the fourth lumbar vertebrae were dissected to remove soft tissue. The posterior elements and endplates of each vertebra were removed with a low speed diamond saw (Buehler Corp., Lake Bluff, IL, USA) and bone marrow was washed out using a low-pressure water jet. Vertebrae were fixed in 10% buffered formalin and embedded undecalcified in opaque methyl-methacrylate.

Three-dimensional images of each specimen were collected using serial block face imaging implemented through fully-automated serial milling. We present a brief description of the approach here, but refer the reader to prior publications for additional details [14,15]. Serial milling involves repeatedly trimming away (destructively) the top of a specimen and collecting a mosaic of images of the newly revealed surface. The images are then stitched together and stacked to achieve three-dimensional images of each specimen at a resolution of 0.7 × 0.7 × 5.0 micrometers per voxel. Three images of each specimen cross-section were collected using different fluorescent filter sets: one channel to visualize bone tissue autofluorescence (UV filter set 350/420 nm, Ex/Em), one channel to visualize xylenol orange formation labels (TRITC, 545/620 nm) and one channel to visualize calcein formation labels (FITC, 470/525 nm). The differences in excitation/emission wavelengths ensure minimal overlap of fluorescent signal among images. Each raw three-dimensional image of a vertebra (6 × 4 × 5 mm in size) was acquired over 5 days (fully automated acquisition). Images of each specimen consisted of 1000 cross-sections using a 4 × 3 array of image tiles (a total of 36,000 individual images per specimen). The raw images occupied 98 GB of memory per fluorescent channel (294 GB total per specimen). Raw images were transferred to a workstation for processing.

Image Processing and Validation

Image processing to segment bone autofluorescence involved the following steps [15]: automatic tiling to create a mosaic of the images from each cross-section; vertical alignment of individual cross-sections using a fiduciary marker; subtraction of out of plane signal; and segmentation of bone using a local iterative thresholding algorithm. We have shown that this image processing approach allows for visualization of small bone surface features enabling tracing of individual resorption cavities (identified as eroded surfaces) [16]. Due to the large size of the image data, image processing required 5 days of computational time per

specimen (Dell Precision T5400, 32GB RAM, 2.66GHz processor with 1333 MHz front side bus). The fully processed image of the bone in each rat vertebra was reduced to approximately 9 GB of segmented data in binary (single bit per voxel) format.

Xylenol orange and calcein image data were stitched together using positioning information from the bone channel and processed as follows: Serial block face imaging is subject to fluorescence signal originating from below the surface. Out-of-plane signal blurs the edges of features in raw images, thereby exaggerating feature size upon segmentation. Out-of-plane signal was removed by subtracting the attenuated and convolved underlying image (the so-called "Next Image" method) [15,24]. Serial block face imaging is also susceptible to cutting marks left on the newly revealed specimen block face. Grayscale morphological closing with a disk shaped structuring element was applied to fill gaps in pixel intensity caused by cutting marks. Each image volume was then resampled to produce approximately isotropic voxels (1.4 × 1.4 × 1.7 μm/voxel). Segmentation was achieved using manually determined global thresholds for each fluorescence channel. Subsequently, three-dimensional binary morphological closing with a spherical structuring element (5.6 μm in radius) was applied to reconnect labels that were discontinuous due to cutting artifacts. Fluorescence signal from within the marrow space was removed by applying a mask of the thresholded bone volume. The resulting image displayed formation labels within bone as well as a number of small noise specks. Objects less than 10,000 μm^3 (the volume of ~14 osteoblasts, much smaller than the 2,300 osteoblasts that make up one formation site [7,25]) were classified as noise and were removed from the image, providing a fully processed image of the formation labels (Fig. 1C–D). Image processing and visualization were performed using custom software written with Matlab (R2008a with Image Processing Toolbox, Natick, MA, USA) and scripts written for Amira (5.3 Visage Imaging, San Diego, CA, USA).

Validation of fluorescent bone formation label segmentation was achieved through pixel-by-pixel comparison to manual tracing (Fig. 1A). Cross-sections of the raw images (5 per specimen) were chosen using systematic random sampling. 'Next-image' processing was applied, but no other pre-processing was performed prior to manual tracing, thereby simulating examination of histology slides. The user then traced each formation label observed in the image using a mouse (mimicking tracing using semi-automated histomorphometry systems). Errors in thresholding were expressed in terms of false positives (Type I error) and false negatives (Type II error) assuming objects traced by the user to be entirely accurate. Type I error was quantified as the cross-sectional area of objects not identified by the observer relative to the cross-sectional area of objects traced by the observer. Type II error was quantified as the ratio of total arc length of tracing lines not contained in the final three-dimensional image relative to the total arc length of all tracing lines created by the observer. Sensitivity was expressed as the arc length of false negatives divided by the sum of arc lengths for true positives and false negatives.

Three-Dimensional Measurements of Bone Remodeling

Resorption cavities were identified by a trained observer as an indentation in the three-dimensional image of the bone surface and confirmed by observing an irregular bone surface texture (the so-called scalloped surface) in the original gray-scale images [16]. All observable cavities were manually traced on the surface of the three-dimensional image by outlining the edge of each cavity with the lasso tool in the Amira surface editing module (Fig. 2A, B). Next, measures of resorption cavity depth, volume, and total volume occupied by cavities were determined. A three-dimensional cubic spline was fit to the outer 50 μm of bone surface surrounding each manually traced cavity (spline fits were insensitive to the selection of 50 μm of surrounding bone; altering the distance to 40 μm changed measures of maximum cavity depth by less than 2% on average). The cubic spline surface was generated

with Lagrangian end conditions such that the slope of the spline matched that of the three-dimensional bone surface immediately surrounding the resorption cavity. The spline surface spanned the resorption cavity, thereby approximating the 'pre-resorbed' bone surface (Fig. 2C, D). Maximum cavity depth was determined as the maximum distance between the 'pre-resorbed' bone surface and the eroded surface within the cavity. Mean cavity depth was determined as the mean distance between the 'pre-resorbed' bone surface and the eroded surface within the cavity. Volume per cavity was determined by measuring the volume enclosed by the 'pre-resorbed' bone surface and eroded surface (Fig. 2E).

Three-dimensional measures of mineral apposition rate were achieved by determining the volume of bone between a pair of bone formation labels (one xylenol orange and another calcein), referred to here as a "double labeled formation event" (dL.Ev) (Fig. 1B, Supplemental Fig. 1). An automated method was required to identify all pairs of complimentary formation labels. A limit on the search radius for complimentary labels was imposed to avoid considering two very distant labels as a pair. Double labeled formation events were comprised of xylenol orange and calcein labels within 8 voxels of each other (this distance corresponded to 11.3 μm, the 95th percentile of inter-label distance expected for this labeling strategy [17,26]). A custom written algorithm was used to 'flatten' the formation labels into a one voxel thick surface through the midline of the object, mimicking the label centerlines used for tracing formation labels in traditional dynamic bone histomorphometry [27]. Mineral apposition rate determined in three-dimensional images (3DMAR) was expressed by dividing the volume of bone between the flattened formation surfaces by the formation event's cross-sectional area and interlabel injection time (μm^3 bone formed/μm^2 event surface area/day, Supplemental Fig. 1).

The three-dimensional measures of bone resorption presented here include measures of percent eroded surface (ES/BS), the number of resorption cavities per unit bone surface (N.Cv/BS, $1/mm^2$), bone surface area per cavity (BS/Cv, μm^2), maximum resorption depth per cavity (Cv.De, μm), mean resorption depth per cavity, volume occupied by each cavity (Cv.V, μm^3) and total volume occupied by resorption cavities (presented relative to bone volume, Tt.Cv.V/BV). Three-dimensional measures of bone formation include the number of single and double labeled formation events (N.sL.Ev, N.dL.Ev), surface area per single and double labeled formation event (MS/sL.Ev, MS/dL.Ev), and mineral apposition rate (3DMAR). Following standard sampling rules, counts of objects (resorption cavities, double labeled formation events, etc.) included only those along three of the six boundaries of the region of interest (in this case, cranial, left, or dorsal boundaries) (11,28). All objects present in their entirety (i.e. not in contact with any boundary) were used to measure object surface area, volume or depth (in the case of cavities). All surfaces (whether in contact with the edge of the sampling volume or not) were included in percent surface area measures (ES/BS, dLS/BS, etc.).

Intra-specimen and Inter-Observer Variation

As with traditional histomorphometry, the location and size of the region of interest examined influence measures of remodeling [28]. To understand the effects of region of interest location and size, three adjacent regions of interest, each 1 mm^3 in size, were selected along the cranial-caudal axis of vertebral cancellous bone (Fig. 1C–D, Fig. 3, Supplemental Fig. 2). In addition to examining measurements made within each 1 mm^3, the regions were combined to create 2 mm^3 and 3 mm^3 regions of interest within each vertebral body (3 mm^3 constituted approximately 60% of the entire cancellous bone volume within a vertebra). Differences in three-dimensional measures of resorption cavities, double labeled formation events, and mineral apposition rate among each region of interest were determined using paired t-tests followed by Holm tests for multiple comparisons.

Inter-observer variation in measures of resorption cavity surface area and number has previously been established to be less than 10% of the total variance [16]. Inter-observer variation associated with selection of global thresholds for the fluorescent labels was evaluated by separating measured variance in 3D mineral apposition rate and double labeled bone surface into that between observers and among specimens using ANOVA [29,30]. Differences in cavity and formation label morphology between groups were determined using a generalized least squares model with random effects (REML) to account for multiple measurements per animal (i.e. multiple remodeling events per animal) [31]. Statistical analyses were performed using JMP (8 SAS, Cary, NC, USA).

Results

Image Processing Validation

There was strong agreement between manual tracing of fluorescent markers of bone formation and the final segmentation achieved using user-defined global thresholding. On average, formation label cross-sectional area in the semi-automated segmentation was 99.8% of that achieved with manual tracing. Sensitivity was 98.6 ± 0.40% (xylenol orange, mean ± SD, n=5) and 97.6 ± 1.64% (calcein, n=5). Measures that can be achieved in two-dimensional histomorphometry (ES/BS, dLS/BS, MAR) were similar to those obtained within the three-dimensional images (Table 1). Variance between observers accounted for less than 10% of the total observed variance.

When viewed in three-dimensions, individual formation labels have a morphology resembling a “potato chip” (Fig. 1B, Supplemental Fig. 1). Formation labels were situated directly below the bone surface and followed the contours of trabeculae. Formation labels were typically 200 × 200 × 15 μm in size. However, some formation labels exceeded 2 mm in greatest dimension with respect to the x-y-z directions. On average, each specimen contained one or two labels with a dimension greater than 2 mm. Often these outliers intersected the boundaries of the region of interest and could not be included in measures of the formation event size because they were not entirely within the region of interest (but they were included in measures of formation event number and percent surface area, see Methods above). Outliers that were completely within the boundaries of some specimens were not found to bias measures of average formation event size. The amount of xylenol orange formation label (measured as total surface area) and the amount of calcein formation label were similar (within 1.5% of each other by surface area). Both isolated formation labels (single labeled) and paired (a double labeled formation event) were observed. On the order of half of the resorption cavities in each specimen were near a double labeled or single labeled formation event, as would be expected from the hemi-osteonal theory of bone remodeling. Consistent with the theory of hemi-osteonal remodeling, resorption cavities were also present without neighboring formation labels (presumably a basic multicellular unit that had recently originated). Additionally we observed double labeled or single labeled formation events without a neighboring resorption cavity (presumably a basic multicellular unit that is terminating).

Region of Interest Size

As expected, as the size of the region of interest was increased, the resulting histomorphometry measurements converged. No significant differences in cavity area, 3D mineral apposition rate, or the area of double labeled formation events were observed between 1 mm^3, 2 mm^3, and 3 mm^3 regions of interest (Fig. 3, Supplemental Fig. 2). Measures obtained in 2 mm^3 regions of interest were within 12% of the value obtained with a 3 mm^3 region of interest (Table 2, 3, Supplemental Figure 2) suggesting that 2 mm^3 is sufficient sampling for three-dimensional dynamic histomorphometry measurements in rat

bone. Results from entire 3 mm^3 regions of interest are reported to take advantage of all available data.

Alterations in 3D Measures of Bone Resorption and Formation Associated with Established Ovariectomy

Established ovariectomy-induced estrogen depletion was associated with a significantly less bone volume fraction and increased percent eroded surface (ES/BS) as compared to sham operated animals (Table 2). Number of cavities per unit bone surface and total volume occupied by resorption cavities were greater in the OVX group (Table 2). No significant differences in average cavity surface area, mean cavity depth, maximum cavity depth, or cavity volume were observed between groups. However, the total volume occupied by resorption cavities was larger in the OVX group ($p < 0.001$). Three-dimensional mineral apposition rate was normally distributed across all formation events and did not differ between OVX and sham groups (Table 3). Double labeled bone surface (dLS/BS) was, on average, 23% greater in OVX than in sham specimens ($p < 0.05$, Table 3). The amount of single labeled bone surface (sLS/BS) was small and did not differ between groups. Mineralizing surface as determined traditionally (dLS/BS + 1/2 sLS/BS) was greater in the OVX group (15.5 ± 2.37%) than in the sham group (12.2 ± 1.41%, $p < 0.05$). Cavity size and double labeled formation event size were skewed, but not significantly different from a normal distribution (Shapiro-Wilk test for normality, Fig. 4). In ovariectomized animals, the number of double labeled formation events per unit bone surface was reduced, but the surface area per double labeled formation event (MS/dL.Ev) was increased ($p < 0.05$).

Discussion

We have demonstrated a new three-dimensional approach to achieving measures of bone remodeling at the level of individual remodeling events. In addition to achieving measures of percent surface area similar to those achieved using traditional two-dimensional histomorphometry, the three-dimensional approach provides a host of new ways to examine bone remodeling including the number and size of individual resorption cavities and bone forming sites (double labeled formation events). Using two-dimensional techniques, it is well known that established ovariectomy in the rat displays a greater proportion of the bone surface undergoing resorption and formation than in estrogen replete animals. The current three-dimensional approach shows that increases in bone resorption and formation in established ovariectomy occur through an increase in number of resorption cavities per unit bone surface with no significant difference in surface area, cavity depth (both maximum depth and mean depth), or volume per resorption cavity. Additionally, established ovariectomy is characterized by a reduction in the number of double labeled formation events per unit bone surface and a corresponding increase in surface area per double labeled formation event.

There are a number of strengths of the current approach that give us confidence in our conclusions. First, the detection of resorption cavities utilized two methods: observation of an indentation on the bone surface in a three-dimensional image followed by confirmation of the scalloped surface in two-dimensional cross-sections (the approach used in conventional histomorphometry) [16]. Additionally, validation of the bone formation label processing was performed through pixel-by-pixel comparison to manual tracing by a trained observer and resulted in sensitivity in excess of 97%, suggesting that measurements based on fluorescent markers are not biased by the image processing approach. Furthermore, the histomorphometry measures that can be performed in both two- and three-dimensional images were similar and followed the patterns of prior studies of established ovariectomy in similarly aged rats. For example, percent double labeled surface (14.2 ± 2.15%, OVX in the current study), was within the range of mineralizing surface values reported in prior studies

(13.1% – 37.9%) [17,18,32]. Three-dimensional measures of mineral apposition rate (1.01 ± 0.46 μm/day) were also within the range of values previously reported using the two-dimensional approach (0.60 – 2.50 μm/day) [17,33–35]. Finally, in traditional dynamic histomorphometry, mineralizing surface is calculated as double labeled surface plus one half single labeled surface. Single labeled surface is included to correct for label escape error when determining mineral apposition rate [36]. The number of single labeled events per unit bone surface was highly variable from specimen to specimen. Such irregularities are reasonable because it is unlikely that all osteoblasts at a remodeling site initiate or terminate matrix formation simultaneously, resulting in an array of small patches of bone formation label. Lastly, while prior studies have reported two-dimensional methods of measuring resorption cavity depth and erosion depth by estimating the pre-resorbed bone surface, the current study is the first to demonstrate such a technique in a three-dimensional image. It is expected that our approach is more accurate than previous two-dimensional approaches as the surface interpolation is in three-dimensions, accounting for cavity morphology out of plane. An additional novelty of our three-dimensional approach is the ability to measure cavity volume and the total volume occupied by resorption cavities.

There are, however, a few limitations to the current study. First, because it is not yet possible to directly view osteoclasts using this imaging modality, resorption cavities were identified based solely on bone surface irregularities (the so-called “scalloped surface”), and are therefore characterized as “eroded surfaces.” Although eroded surface is not a direct measure of active resorption, it is an accepted measure commonly used in histomorphometry. Furthermore, any biomechanical effects of resorption cavities will be present whether or not active resorption is occurring on an eroded surface. Second, the current study addresses only the state of bone remodeling after established ovariectomy in the rat. Prior studies have indicated that in the few weeks following ovariectomy surgery there is a transient increase in bone turnover [21]. It is possible the early reaction to ovariectomy surgery is associated with changes in bone remodeling events that were not observed here. While the current study does not address the early response to ovariectomy, it does address the condition of established estrogen depletion, which is a common pre-treatment condition in animals and humans.

It has long been known that established estrogen depletion would show increases in percent eroded surface as compared to estrogen replete animals. Here we have provided the first quantitative measures of resorption cavity morphology showing that established ovariectomy in the rat is associated with increased number of resorption cavities and total volume occupied by cavities. Only small differences in average cavity surface area (15%), mean cavity depth (6%), and maximum cavity depth (6%) were observed between groups. Post-hoc power analysis suggests that the current study was capable of detecting a 25% difference in average cavity surface area (power = 0.89, $\alpha = 0.05$), a 35% difference in maximum cavity depth (power = 0.80, $\alpha = 0.05$), and a 31% difference in cavity volume (power = 0.83, $\alpha = 0.05$) suggesting that, if these parameters are altered in established ovariectomy, the difference is modest.

Although we observed a decrease in number and increase in size of double labeled formation events in established ovariectomy, we believe that these differences are not caused by alterations in BMU size, but are instead due to formation events from different BMUs merging with one another. There are a number of reasons that we believe the apparent merging of formation events is not an artifact of the image processing methodology. First, the percent eroded and forming surfaces are similar to the literature and the formation label processing is highly sensitive (see above). Second, although morphological processing was used to bridge small patches of bone formation labels for enumeration, our morphological processing approach only bridged patches of fluorescent

label separated by 5.6 μm, a distance that is smaller than a single osteoblast. Active osteoblasts within 5.6 μm of one another are likely to experience the same chemical microenvironment, they are effectively functioning as a single formation event [37]. It is likely that merging of formation events was more pronounced in established ovariectomy due to the combined increase in bone turnover and reduction in bone surface. Because the larger and less numerous double labeled formation events in OVX animals appear to be due to merging of formation events from different BMUs, the current study does not support the idea that established ovariectomy is associated with alterations in bone formation beyond that associated with coupling to osteoclastic resorption.

Our three-dimensional approach has the potential to improve our understanding of the connection between in vitro cell culture and in vivo cell activity in the form of BMUs. Basic multicellular units in cancellous bone are believed to form a hemi-osteon, consisting of active bone resorption with neighboring new bone formation, although visualization of such hemi-osteons is rare in histology sections [38]. In the current study, we observed many remodeling events consisting of a formation surface with a neighboring cavity, consistent with the hemi-osteonal theory of bone remodeling. Additionally, in vitro and in vivo studies suggest that estrogen depletion has been associated with increases in osteoclast precursor number and differentiation as well as decreases in osteoclast apoptosis [2,20,39–44]. While increases in osteoclast differentiation presumably lead to an increase in the number of resorption cavities, it has been suggested that reductions in osteoclast apoptosis allow osteoclasts to progress further along or into the bone surface, thereby increasing the surface area or depth of each resorption cavity [45]. Our finding that established ovariectomy is associated with increased number of resorption cavities per unit bone surface is consistent with the idea of increased osteoclast differentiation/proliferation. The fact that resorption cavities are not larger in surface area or depth suggests that if there are alterations in osteoclast apoptosis in this in vivo model of established ovariectomy they do not greatly influence cavity morphology. If our interpretation above is correct and established ovariectomy is not associated with changes in bone formation beyond those secondary to increased osteoclast activity, it would support the idea that the primary effect of prolonged reductions in circulating estrogens on bone remodeling is on the proliferation and differentiation of osteoclast precursors, i.e. the origination rate of new BMUs, and not on BMUs once they are active.

The three-dimensional approach to dynamic histomorphometry described here provides novel improvements over traditional histomorphometry. The degree of automation in the image acquisition approach greatly reduces labor requirements. Additionally, because measures are performed on digital images, the approach has the potential to reduce intra-laboratory and inter-laboratory variability in remodeling indices. Lastly, the three-dimensional nature of the approach allows for measures of remodeling event number and size. The size and depth of resorption cavities have the potential to influence local tissue stresses, altering the mechanotransduction of local bone cells and potentially influencping failure or failure processes in cancellous bone. Further advancements with this approach include three-dimensional measures of origination frequency (which would be independent of bone formation rate), three-dimensional measures of bone balance, and spatial correlations between new bone formation and trabecular microstructure and/or mechanical stresses and strains.

Supplementary Material

Refer to Web version on PubMed Central for supplementary material.

Acknowledgments

Funding Sources: Funding for this study was provided by the National Institutes of Health/National Institute of Arthritis and Musculoskeletal and Skin Diseases R21AR054448, T32 AR007505–22 (C.R.S.)

The authors thank Kathy Tinoco and Ralph O'Brien. This work was supported by NIH/NIAMS R21AR054448, T32 AR007505–22 (C.R.S.), and Cornell University. Dr. Wilson has an interest in BioInVision, Inc., which may commercialize the serial milling technology.

References

1. Frost HM. Bone dynamics in metabolic bone disease. J Bone Joint Surg. 1966; 48(6):1192. [PubMed: 5331235]
2. Parfitt AM, Mundy GR, Roodman GD, Hughes DE, Boyce BF. A new model for the regulation of bone resorption, with particular reference to the effects of bisphosphonates. J Bone Miner Res. 1996; 11(2):150–9. [PubMed: 8822338]
3. Parfitt AM. Misconceptions (2): turnover is always higher in cancellous than in cortical bone. Bone. 2002; 30(6):807–9. [PubMed: 12052445]
4. Seeman E, Delmas PD. Bone Quality — The Material and Structural Basis of Bone Strength and Fragility. New Eng J Med. 2006; 354(21):2250–2261. [PubMed: 16723616]
5. Hernandez CJ. How can bone turnover modify bone strength independent of bone mass? Bone. 2008; 42(6):1014–1020. [PubMed: 18373970]
6. Kummari S, Coan T, Hernandez C. Stress Concentration Factors of Remodeling Cavities on Rod-like and Plate-like Trabeculae Orth Res Soc. 2011
7. Parfitt, AM. The physiologic and clinical significance of bone histomorphometric data. In: Recker, RR., editor. Bone histomorphometry: techniques and interpretation. CRC Press; Boca Raton, FL: 1983. p. 143-223.
8. Compston, J. Bone histomorphometry. In: Arnett, T., editor. Methods in bone biology. 1. Chapman & Hall; London: 1997. p. 177-197.
9. Parfitt AM, Drezner MK, Glorieux FH, Kanis JA, Malluche H, Meunier PJ, Ott SM, Recker RR. Bone histomorphometry: standardization of nomenclature, symbols, and units. Report of the ASBMR Histomorphometry Nomenclature Committee. J Bone Miner Res. 1987; 2(6):595–610. [PubMed: 3455637]
10. Hauge EM, Mosekilde L, Melsen F. Stereological considerations concerning the measurement of individual osteoid seams and resorption cavities. J Bone Miner Res. 1994; 26 (1):89–90.
11. Howard, CV.; Reed, MG. Unbiased Stereology: Three Dimensional Measurement in Microscopy. Springer-Verlag; New York, NY: 1998.
12. Odgaard A, Andersen K, Melsen F, Gundersen HJ. A direct method for fast three-dimensional serial reconstruction. J Microsc. 1990; 159:335–342. [PubMed: 2243366]
13. Beck JD, Canfield BL, Haddock SM, Chen TJ, Kothari M, Keaveny TM. Three-dimensional imaging of trabecular bone using the computer numerically controlled milling technique. Bone. 1997; 21(3):281–7. [PubMed: 9276094]
14. Kazakia GJ, Lee JJ, Singh M, Bigley RF, Martin RB, Keaveny TM. Automated high-resolution three-dimensional fluorescence imaging of large biological specimens. J Microsc. 2007; 225(Pt 2): 109–17. [PubMed: 17359245]
15. Slyfield CR Jr, Niemeyer KE, Tkachenko EV, Tomlinson RE, Steyer GG, Patthanacharoenphon CG, Kazakia GJ, Wilson DL, Hernandez CJ. Three-dimensional surface texture visualization of bone tissue through epifluorescence-based serial block face imaging. J Microsc. 2009; 236(1):52–9. [PubMed: 19772536]
16. Tkachenko EV, Slyfield CR, Tomlinson RE, Daggett JR, Wilson DL, Hernandez CJ. Voxel size and measures of individual resorption cavities in three-dimensional images of cancellous bone. Bone. 2009; 45(3):487–92. [PubMed: 19482097]
17. Li CY, Jee WS, Chen JL, Mo A, Setterberg RB, Su M, Tian XY, Ling YF, Yao W. Estrogen and "exercise" have a synergistic effect in preventing bone loss in the lumbar vertebra and femoral neck of the ovariectomized rat. Calcif Tissue Int. 2003; 72(1):42–9. [PubMed: 12370795]

18. Jee WSS, Tang L, Ke HZ, Setterberg RB, Kimmel DB. Maintaining restored bone with bisphosphonate in the ovariectomized rat skeleton: Dynamic histomorphometry of changes in bone mass. Bone. 1993; 14(3):493–498. [PubMed: 8363898]
19. Riggs BL, Parfitt AM. Drugs Used to Treat Osteoporosis: The Critical Need for a Uniform Nomenclature Based on Their Action on Bone Remodeling. J Bone Miner Res. 2005; 20 (2):177–184. [PubMed: 15647810]
20. Parfitt, AM. Skeletal Heterogeneity and the Purposes of Bone Remodeling: Implications for the Understanding of Osteoporosis. In: Marcus, R.; Feldman, D.; Nelson, D.; Rosen, C., editors. Osteoporosis. 3. Vol. 1. Academic Press; 2008.
21. Wronski TJ, Dann LM, Scott KS, Cintrón M. Long-term effects of ovariectomy and aging on the rat skeleton. Calcif Tiss Int. 1989; 45(6):360–366.
22. Parfitt AM. Trabecular bone architecture in the pathogenesis and prevention of fracture. Am J Med. 1987; 82(1B):68–72. [PubMed: 3544835]
23. van der Linden JC, Verhaar JA, Weinans H. A three-dimensional simulation of age-related remodeling in trabecular bone. J Bone Miner Res. 2001; 16(4):688–96. [PubMed: 11315996]
24. Steyer GJ, Roy D, Salvado O, Stone ME, Wilson DL. Removal of out-of-plane fluorescence for single cell visualization and quantification in cryo-imaging. Ann Biomed Eng. 2009; 37(8):1613–1628. [PubMed: 19513848]
25. Marotti G, Zallone A, Ledda M. Number, size and arrangement of osteoblasts in osteons at different stages of formation. Calcif Tiss Int. 1975; 21(1):96–101.
26. Evans G, Bryant HU, Magee D, Sato M, Turner RT. The effects of raloxifene on tibia histomorphometry in ovariectomized rats. Endoc. 1994; 134(5):2283–2288.
27. Recker, RR. Bone histomorphometry: techniques and interpretation. CRC Press; Boca Raton, Fla: 1983.
28. Bouxsein ML, Boyd SK, Christiansen BA, Guldberg RE, Jepsen KJ, Müller R. Guidelines for assessment of bone microstructure in rodents using micro–computed tomography. J Bone Miner Res. 2010; 25(7):1468–1486. [PubMed: 20533309]
29. Eriksen EF, Melsen F, Mosekilde L. Reconstruction of the resorptive site in iliac trabecular bone: a kinetic model for bone resorption in 20 normal individuals. Metab Bone Dis Relat Res. 1984; 5(5): 235–42. [PubMed: 6493035]
30. Hauge EM, Mosekilde L, Melsen F, Frydenberg M. How many patients are needed? Variation and design considerations in bone histomorphometry. Bone. 2001; 28(5):556–62. [PubMed: 11344056]
31. Kopperdahl DL, Morgan EF, Keaveny TM. Quantitative computed tomography estimates of the mechanical properties of human vertebral trabecular bone. J Orth Res. 2002; 20 (4):801–805.
32. Bagi CM, Brommage R, Deleon L, Adams S, Rosen D, Sommer A. Benefit of systemically administered rhIGF I and rhIGF I/IGFBP 3 on cancellous bone in ovariectomized rats. J Bone Miner Res. 1994; 9(8):1301–1312. [PubMed: 7526611]
33. Dobnig H, Turner RT. Evidence that intermittent treatment with parathyroid hormone increases bone formation in adult rats by activation of bone lining cells. Endoc. 1995; 136(8):3632–8.
34. Schmidt I, Dobnig H, Turner R. Intermittent parathyroid hormone treatment increases osteoblast number, steady state messenger ribonucleic acid levels for osteocalcin, and bone formation in tibial metaphysis of hypophysectomized female rats. Endoc. 1995; 136(11):5127.
35. Meng XW, Liang XG, Birchman R, Wu DD, Dempster DW, Lindsay R, Shen V. Temporal expression of the anabolic action of PTH in cancellous bone of ovariectomized rats. J Bone Miner Res. 1996; 11(4):421–429. [PubMed: 8992872]
36. Frost, HM. Bone histomorphometry: Correction of the labelling “escape error”. In: Recker, RR., editor. Bone Histomorphometry: Techniques and Interpretation. CRC Press; Boca Raton, FL: 1983. p. 133-142.
37. Bell KL, Loveridge N, Reeve J, Thomas CDL, Feik SA, Clement JG. Super-osteons (remodeling clusters) in the cortex of the femoral shaft: Influence of age and gender. Anat Rec. 2001; 264(4): 378–386. [PubMed: 11745093]
38. Parfitt AM. Osteonal and hemi-osteonal remodeling: the spatial and temporal framework for signal traffic in adult human bone. J Cell Biochem. 1994; 55(3):273–86. [PubMed: 7962158]

39. Jilka R, Hangoc G, Girasole G, Passeri G, Williams D, Abrams J, Boyce B, Broxmeyer H, Manolagas S. Increased osteoclast development after estrogen loss: mediation by interleukin-6. Science. 1992; 257(5066):88. [PubMed: 1621100]
40. Jilka RL, Passeri G, Girasole G, Cooper S, Abrams J, Broxmeyer H, Manolagas SC. Estrogen loss upregulates hematopoiesis in the mouse: a mediating role of IL-6. Exp Hemat. 1995; 23(6):500. [PubMed: 7768305]
41. Kimble RB, Srivastava S, Ross FP, Matayoshi A, Pacifici R. Estrogen deficiency increases the ability of stromal cells to support murine osteoclastogenesis via an interleukin-1and tumor necrosis factor-mediated stimulation of macrophage colony-stimulating factor production. J Bio Chem. 1996; 271(46):28890. [PubMed: 8910536]
42. Hughes DE, Dai A, Tiffee JC, Li HH, Mundy GR, Boyce BF. Estrogen promotes apoptosis of murine osteoclasts mediated by TGF-[beta]. Nat Med. 1996; 2(10):1132–1136. [PubMed: 8837613]
43. Romas E, Udagawa N, Zhou H, Tamura T, Saito M, Taga T, Hilton DJ, Suda T, Ng KW, Martin TJ. The role of gp130-mediated signals in osteoclast development: Regulation of interleukin 11 production by osteoblasts and distribution of its receptor in bone marrow cultures. J Exp Med. 1996; 183(6):2581–2591. [PubMed: 8676079]
44. Nakamura T, Imai Y, Matsumoto T, Sato S, Takeuchi K, Igarashi K, Harada Y, Azuma Y, Krust A, Yamamoto Y, Nishina H, Takeda S, Takayanagi H, Metzger D, Kanno J, Takaoka K, Martin TJ, Chambon P, Kato S. Estrogen prevents bone loss via estrogen receptor alpha and induction of Fas ligand in osteoclasts. Cell. 2007; 130(5):811–823. [PubMed: 17803905]
45. Parfitt AM, Mundy GR, Roodman GD, Hughes DE, Boyce BF. Theoretical perspective: A new model for the regulation of bone resorption, with particular reference to the effects of bisphosphonates. J Bone Miner Res. 1996; 11(2):150–159. [PubMed: 8822338]

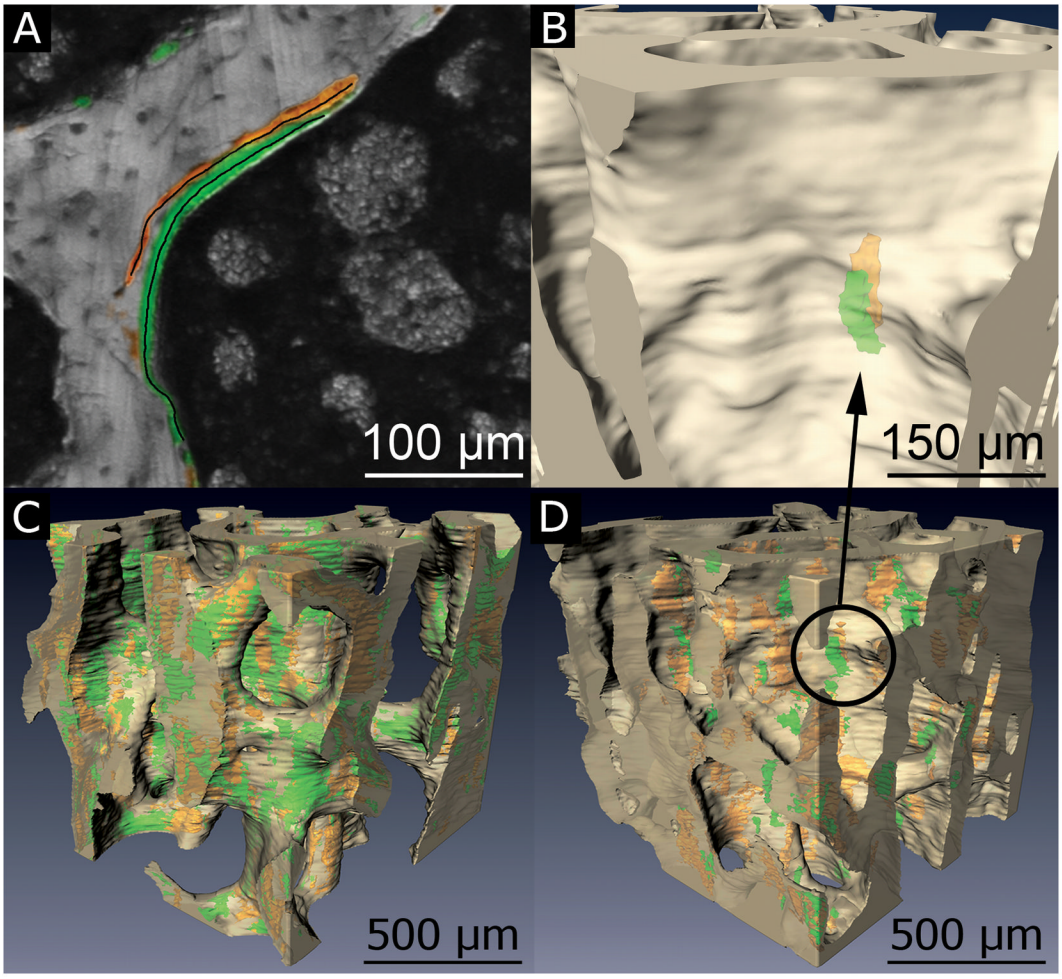

Fig. 1.

(A) Image processing is validated through direct comparison of pixels in the traced labels to corresponding pixels in automatically processed images. **(B)** A double labeled formation event, consisting of a pair of spatially correlated formation labels (xylenol orange, calcein green), is visible by making the bone surface partially transparent. Images of bone tissue (off-white) and fluorescent bone formation labels (xylenol orange, calcein green) are shown for **(C)** ovariectomized (OVX) and **(D)** sham operated animals.

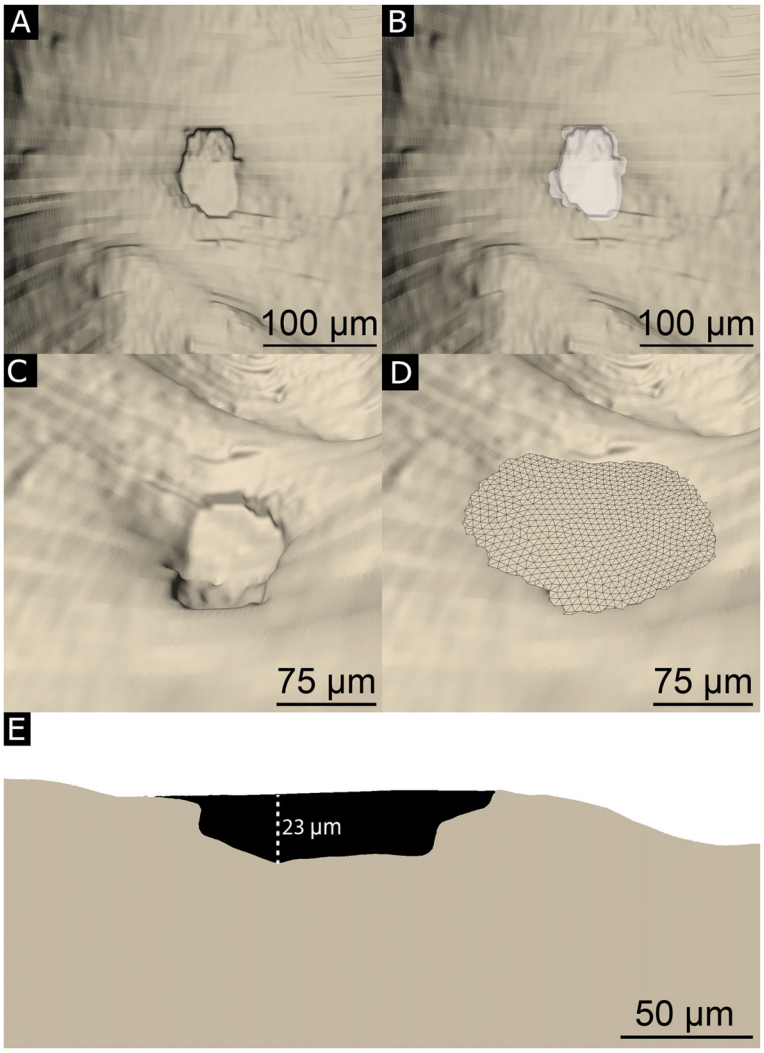

Fig. 2.

(A) Resorption cavities are identified as indentations on the bone surface. The horizontal lines that appear on the reconstructed bone surface correspond to cross-sections during image acquisition. **(B)** An observer manually traces the resorption cavity (white). **(C, D)** Maximum Cavity depth is determined by approximating the 'pre-resorbed' bone surface above a resorption cavity using a three-dimensional spline (see Methods for a description of the curve fitting). **(E)** A cross-section of a resorption cavity with the 'pre-resorbed' surface applied is shown. Cavity depth was measured as the maximum distance between the 'pre-resorbed' surface and the eroded surface (dashed line).

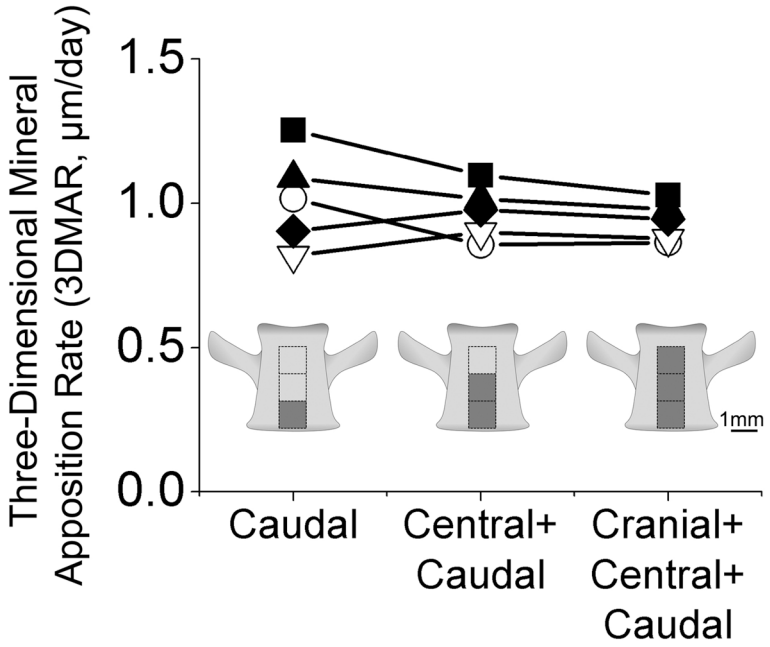

Fig. 3.

Mineral apposition rate in ovariectomized animals (each line is an individual rat) measured in three different regions of interest (caudal, central+caudal, and cranial+central+caudal) are shown illustrating that measurements made in 2 mm^3 regions of interest are similar to those achieved using larger regions of interest.

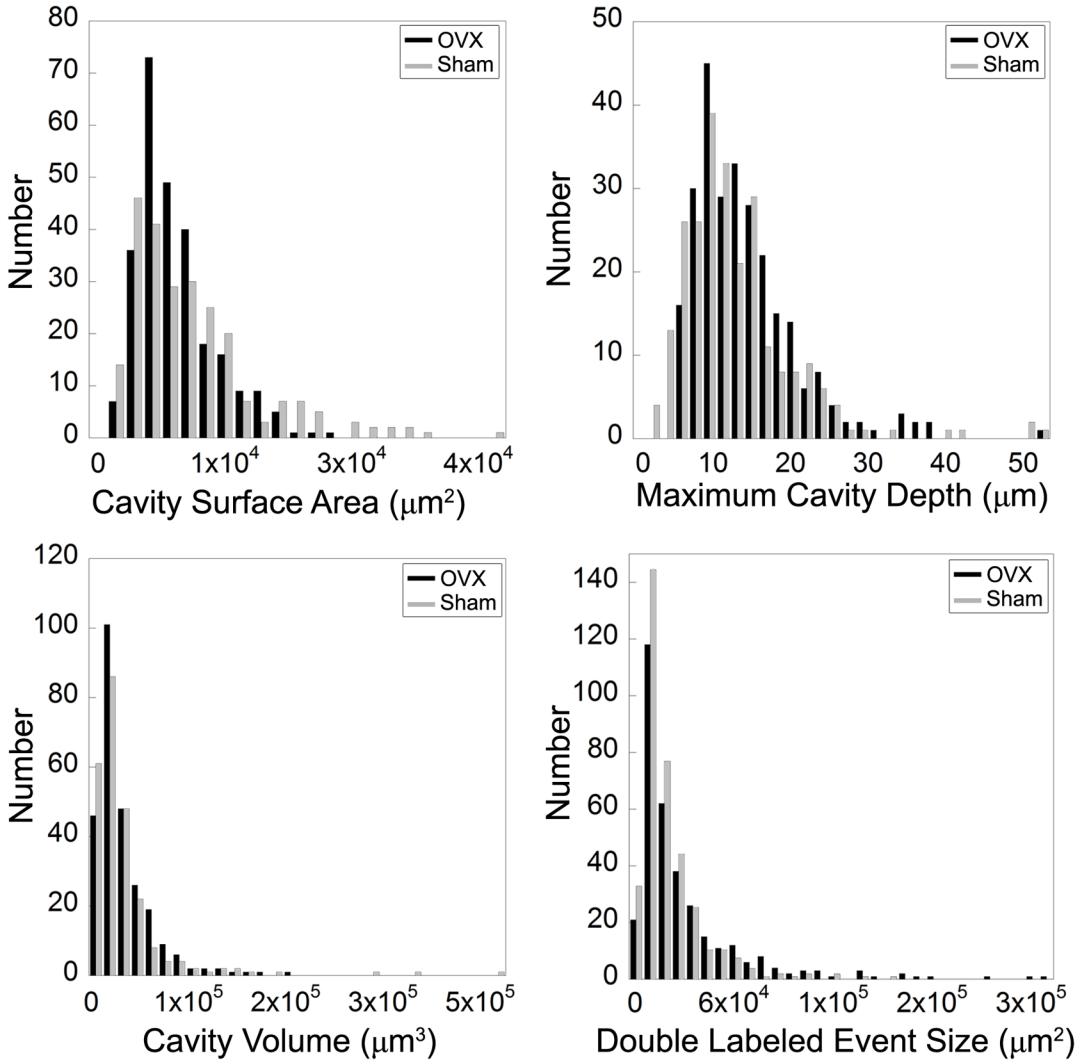

Fig. 4.

Histograms of cavity surface area, maximum cavity depth, cavity volume, and double labeled formation event size are shown. The histograms represent pooled data from all of the specimens examined in the study.

Table 1

Measurements achieved in ovariectomized animals (n=5) using traditional two-dimensional techniques are shown along with three-dimensional measures from the same specimens (mean ± SD). The paired difference between the two approaches is determined within each specimen and the average value across all specimens is shown.

	Two-Dimensional (2D measure)	Three-Dimensional (3D measure)	Paired Difference (2D–3D)/2D*100%
ES/BS (%)	5.01 ± 0.48%	4.79 ± 0.66%	−2.33 ± 8.31%
dLS/BS (%)	10.9 ± 1.79%	14.2 ± 2.15%	1.57 ± 0.19%
MAR (μm/d)	0.92 ± 0.07	0.94 ± 0.44	−3.00 ± 0.06%

Table 2

Static histomorphometric measures made using the three-dimensional approach are shown (mean ± SD, n=5 per group).

	SHAM	OVX
Bone Volume Fraction	31.5 ± 7.52%	19.7 ± 4.0% [a]
Bone Specific Surface (BS/TV, mm^{-1})	29.2 ± 2.20	22.8 ± 2.17 [a]
Trabecular Thickness (Tb.Th, μm)	81.3 ± 8.07	70.5 ± 3.26 [a]
Trabecular Separation (Tb.Sp, μm)	221 ± 41.1	310 ± 30.4 [a]
Structural Modeling Index (SMI)	0.96 ± 0.23	1.38 ± 0.33 [a]
Degree of Anisotropy (DA)	0.68 ± 0.07	0.68 ± 0.49
Percent Eroded Surface	2.54 ± 0.13%	4.79 ± 0.66% [b]
Number of Resorption Cavities (N.Cv)	105 ± 3.96	134 ± 13.6 [b]
Number of Resorption Cavities/BS (N.Cv/BS, mm^{-2})	2.38 ± 0.24	3.86 ± 0.35 [b]
Mean Cavity Resorption Depth (μm)	4.23 ± 1.85	3.99 ± 0.88
Maximum Cavity Resorption Depth (Cv.De, μm)	14.8 ± 2.56	14.0 ± 1.96
Average Cavity Surface Area (BS/Cv, μm^2)	9,720 ± 1,060	11,200 ± 1,850
Average Cavity Volume (Cv.V, μm^3)	36,500 ± 5,350	52,500 ± 13,900
Total Volume Occupied by Resorption Cavities (Tt.Cv.V/BV)	0.38 ± 0.06%	1.12 ± 0.18% [c]

[a] $p<0.05$,

[b] $p<0.01$,

[c] $p<0.001$as compared to the sham operated group

Table 3

Measures of bone formation made using the 3D approach are shown (mean ± SD, n=5 per group).

	SHAM	OVX
3D Mineral Apposition Rate (μm/day)	1.01 ± 0.46	0.92 ± 0.44
Average Surface Area per Double Labeled Event (MS/dL.Ev, μm^2)	23,700 ± 6,890	33,300 ± 7,950[a]
Average Surface Area per Single Labeled Event (MS/sL.Ev, μm^2)	4920 ± 4560	5490 ± 4970
Percent Double Labeled Surface (dLS/BS)	11.5 ± 0.74%	14.2 ± 2.15%[a]
Percent Single Labeled Surface (sLS/BS)	3.64 ± 1.72%	2.52 ± 0.55%
Number of Double Labeled Formation Events (N.dL.Ev)	152 ± 41.1	73.8 ± 20.7[a]
Number of Single Labeled Formation Events (N.sL.Ev)	187 ± 89.5	80.0 ± 20.8
Number of Double Labeled Formation Events Per Unit Bone Surface (N.dL.Ev/BS, mm^{-2})	5.15 ± 1.07	3.21 ± 0.63 [a]
Number of Single Labeled Formation Events Per Unit Bone Surface (N.sL.Ev/BS, mm^{-2})	6.39 ± 2.85	3.86 ± 0.56

[a] $p<0.05$ as compared to the sham operated group